Title
Distinct tau PET patterns in atrophy-defined subtypes of Alzheimer's disease.

Journal
Alzheimer's & dementia : the journal of the Alzheimer's Association, 16(2)

ISSN
1552-5260

Authors
Ossenkoppele, Rik
Lyoo, Chul Hyoung
Sudre, Carole H
et al.

Publication Date
2020-02-01

DOI
10.1016/j.jalz.2019.08.201

Peer reviewed

HHS Public Access

Author manuscript

Alzheimers Dement. Author manuscript; available in PMC 2020 February 11.

Published in final edited form as:

Alzheimers Dement. 2020 February ; 16(2): 335–344. doi:10.1016/j.jalz.2019.08.201.

Distinct tau PET patterns in atrophy-defined subtypes of Alzheimer's disease

Rik Ossenkoppele[a,b,*], **Chul Hyoung Lyoo**[c], **Carole H. Sudre**[d,e,f], **Danielle van Westen**[g], **Hanna Cho**[c], **Young Hoon Ryu**[g], **Jae Yong Choi**[h,i], **Ruben Smith**[a], **Olof Strandberg**[a], **Sebastian Palmqvist**[a], **Erik Westman**[j], **Richard Tsai**[k], **Joel Kramer**[k], **Adam L. Boxer**[j], **Maria L. Gorno-Tempini**[k], **Renaud La Joie**[k], **Bruce L. Miller**[k], **Gil D. Rabinovici**[k], **Oskar Hansson**[a,l,**]

[a]Lund University, Clinical Memory Research Unit, Lund, Sweden [b]Alzheimer Center Amsterdam, Department of Neurology, Amsterdam Neuroscience, Vrije Universiteit Amsterdam, Amsterdam UMC, Amsterdam, the Netherlands [c]Department of Neurology, Gangnam Severance Hospital, Yonsei University College of Medicine, Seoul, South Korea [d]School of Biomedical Engineering and Imaging Sciences King's College London, London, United Kingdom [e]Dementia Research Centre, Department of Neurodegenerative Disease, UCL Institute of Neurology, London, United Kingdom [f]Centre for Medical Image Computing, Department of Medical Physics, University College London, United Kingdom [g]Lund University, Diagnostic Radiology, Lund, Sweden [h]Department of Nuclear Medicine, Gangnam Severance Hospital, Yonsei University College of Medicine, Seoul, South Korea [i]Division of RI-Convergence Research, Korea Institute Radiological and Medical Sciences, Seoul, South Korea [j]Division of Clinical Geriatrics, Department of Neurobiology, Karolinska Institute, Care Sciences and Society, Stockholm, Sweden [k]Department of Neurology, University of California San Francisco, Memory and Aging Center, San Francisco, USA [l]Memory Clinic, Skåne University Hospital, Malmö, Sweden

Abstract

Introduction: Differential patterns of brain atrophy on structural magnetic resonance imaging (MRI) revealed four reproducible subtypes of Alzheimer's disease (AD): (1) "typical", (2) "limbic-predominant", (3) "hippocampal-sparing", and (4) "mild atrophy". We examined the neurobiological characteristics and clinical progression of these atrophy-defined subtypes.

Methods: The four subtypes were replicated using a clustering method on MRI data in 260 amyloid-β-positive patients with mild cognitive impairment or AD dementia, and we subsequently tested whether the subtypes differed on [^{18}F]flortaucipir (tau) positron emission tomography, white matter hyperintensity burden, and rate of global cognitive decline.

*Corresponding author. Tel.: +31 20 444 0816; Fax: +31 20 444 0816., r.ossenkoppele@amsterdamumc.nl (R.O.). **Corresponding author. Tel.: +46 46 171000; Fax: +46 46 171000., oskar.hansson@med.lu.se (O.H.).

Supplementary data

Supplementary data related to this article can be found at https://doi.org/10.1016/j.jalz.2019.08.201.

Results: Voxel-wise and region-of-interest analyses revealed the greatest neocortical tau load in hippocampal-sparing (frontoparietal-predominant) and typical (temporal-predominant) patients, while limbic-predominant patients showed particularly high entorhinal tau. Typical patients with AD had the most pronounced white matter hyperintensity load, and hippocampal-sparing patients showed the most rapid global cognitive decline.

Discussion: Our data suggest that structural MRI can be used to identify biologically and clinically meaningful subtypes of AD.

Keywords

Alzheimer's disease; Dementia; Tau; Subtypes; Atrophy; Thickness; Cognition

1. Introduction

Various structural neuroimaging approaches have been used to identify subtypes of Alzheimer's disease (AD) based on patterns of regional atrophy [1–4]. These studies identified reproducible AD subtypes, namely "limbic-predominant", "hippocampal-sparing", "typical" (i.e., a combination of limbic-predominant and hippocampal-sparing) AD, and, to a lesser extent, "mild atrophy" AD [5]. These AD subtypes showed robust associations with age, *APOE* ε4 status, and clinical phenotype [6]. However, the neurobiological features underlying AD subtypes are largely unknown and cannot be explained by amyloid-β (Aβ) pathology because the distribution of Aβ positron emission tomography (PET) retention is virtually the same across AD phenotypes [7]. Capturing this heterogeneity is important because it could enhance our understanding of disease mechanisms, it may improve diagnosis and prognosis, and distinct subtypes might respond differently to future disease-modifying treatments. We therefore aimed to test whether tau PET patterns or white matter hyperintensities (WMH) on MRI are associated with distinct atrophy patterns across 260 Aβ + patients with AD to better understand the disease pathologies underlying this heterogeneity in regional neurodegeneration.

2. Methods

2.1. Participants

We included 260 patients from the Memory Disorder Clinic of Gangnam Severance Hospital (Seoul, South Korea), the Swedish BioFINDER study (www.biofinder.se) at Lund University (Lund, Sweden), and the University of California San Francisco (UCSF) AD Research Center (San Francisco, USA) who underwent [^{18}F]flortaucipir PET between June 2014 and November 2017. All patients were Aβ+ by PET and/or cerebrospinal fluid (see our previous report for details [8]), 83 had mild cognitive impairment (MCI [9]), and 177 had AD dementia [10]. All underwent a medical history and complete neurological examination, brain MRI, and neuropsychological testing. Informed consent was obtained from all participants, and local institutional review boards for human research approved the study.

2.2. Acquisition of PET and MRI data

PET images were acquired using a Biograph mCT PET/computed tomography scanner (Siemens Medical Solutions) in Seoul, Discovery 690 PET scanner (GE medical systems) in BioFINDER, a Biograph 6 Truepoint PET/computed tomography scanner (Siemens Medical Solutions) at Lawrence Berkeley National Laboratory for UCSF patients, after a bolus injection of ~370 MBq (BioFINDER and UCSF) or ~280 MBq (Seoul) of [^{18}F]flortaucipir. PET data were locally reconstructed into 4 × 5-minute frames for the 80- to 100-min interval after injection [11–13]. MRI scans were acquired at 3T on a Discovery MR750 scanner (GE medical systems) in Seoul, 3.0T Tim Trio or Skyra scanner (Siemens Medical Solutions) in BioFINDER, and a 3.0T Tim Trio or Prisma scanner (Siemens Medical Solutions) at UCSF.

2.3. T1-weighted MRI processing

MRI data were centrally processed (at Lund University), using previously reported procedures [8]. Briefly, cortical reconstruction and volumetric segmentation were performed with the FreeSurfer image analyses pipeline version 6.0. T1-weighted images underwent correction for intensity homogeneity, removal of nonbrain tissue, and segmentation into gray matter and white matter. Reconstructed data sets were visually inspected for accuracy, and segmentation errors were corrected.

2.4. [^{18}F]Flortaucipir PET processing

PET images were first resampled to obtain the same image size (128 × 128 × 63 matrix) and voxel dimensions (2.0 × 2.0 × 2.0 mm) across centers. Then, PET images were centrally processed (at Lund University) by previously reported procedures [8]. [^{18}F]Flortaucipir images were motion-corrected using Analysis of Functional NeuroImages's 3dvolreg, time-averaged, and rigidly coregistered to the skull-stripped MRI scan. Voxel-wise standardized uptake value ratio (SUVR) images were created using inferior cerebellar gray matter as the reference region [14]. FreeSurfer (version 6.0, http://surfer.nmr.harvard.edu/) parcellation of the T1-weighted MRI scan was applied to the PET data transformed to subjects' native T1-space to extract mean regional SUVR values for each participant. We calculated mean [^{18}F] flortaucipir SUVR in seven predefined regions of interest (ROIs) including entorhinal cortex, lateral temporal cortex, medial and lateral parietal cortex, occipital cortex frontal cortex, and whole-cortex. Detailed composition of each ROI by FreeSurfer label can be found in Supplementary Table 1. In addition, we performed partial volume correction (PVC) using the Geometric Transfer Matrix approach [15]. We report both PVC (main report) and non-PVC (Supplementary Material) ROI results. For voxel-wise analyses, [^{18}F]flortaucipir images were warped into the Montreal Neurological Institute standard space using the nonlinear transformation calculated by normalizing the T1-weighted MRI scan to the Montreal Neurological Institute 152 1 × 1 × 1 mm^3 template with Advanced Normalization ToolS. Before voxel-wise analyses, images were smoothed with an 8-mm full width at half maximum Gaussian kernel [16].

2.5. Fluid Attenuated Inversion Recovery MRI processing

T2-weighted Fluid Attenuated Inversion Recovery images were available for 259 of 260 subjects and were all manually inspected. We estimated WMH volumes following a

segmentation method described elsewhere [17]. This method builds a Bayesian probabilistic data model based on a Gaussian mixture model with evolving number of components, which is able to account for observation outliers and incorporates anatomical priors and contextual constraints. After convergence of the model, candidate lesion voxels are selected based on their distance to normalcy (i.e., healthy white matter), and resulting connected components are then automatically classified as lesion or artefacts based on their anatomical location. Resulting probabilistic maps are integrated over ROIs (layers and lobes) to calculate WMH volumes.

2.6. Clinical progression

Both retrospective and prospective longitudinal Mini-Mental State Examination (MMSE) scores were used to model changes in global cognition over time. We collected a total of 664 data points from 246 patients; 276 MMSE scores were collected between −1 and +1 year to PET, 182 ≤ 1 year before PET and 206 ≥ 1 year after PET. Of 246 patients with MMSE data available, 182 had had at least two time points of data, with a median of 3 (range: 2 to 8 data points). The mean interval between first and last MMSE assessment was 2.0 ± 1.8 years across all groups and was longer for typical AD (3.2 ± 2.0 years) than that for all other groups (limbic-predominant: 1.7 ± 1.7 years, mild atrophy: 1.6 ± 1.4 years, hippocampal-sparing: 1.3 ± 1.1 years, $P < .001$).

2.7. Procedure for determining atrophy-defined subtypes

In a previously described method [18], established visual MRI rating scales of medial temporal lobe atrophy (MTA), posterior atrophy (PA), and global cortical atrophy-frontal subscale (GCA-F) were used to determine atrophy-defined subtypes. Each visual rating scale score was binarized as “normal” or “abnormal” based on established clinical cut-offs [19], and the combination of the scales resulted in classification into distinct subtypes of AD. For example, abnormal MTA + normal PA/GCA-F = “limbic-predominant,” while normal MTA + abnormal PA and/or GCA-F = “hippocampal-sparing.” Advantages of this method are its computational simplicity and relevance to clinical practice, but the nonautomated procedure (i.e., visual read) and dichotomous data structure (i.e., normal/abnormal) could be considered suboptimal. We aimed to apply a quantitative (clustering) implementation that preserves the simplicity and clinical utility of this method. We therefore calculated the mean surface area–weighted thickness of the entire occipital/parietal cortex and frontal cortex (resembling PA and GCA-F scales, respectively) and total intracranial volume–weighted hippocampal volumes (resembling MTA scale). The continuous measures for these three variables were entered into a two-step clustering algorithm in SPSS version 22.0 (Fig. 1A). In the first step, we performed a sequential clustering approach by constructing a modified cluster feature tree using model-based distance criterion (i.e., the decrease in log-likelihood when merging two clusters into one [20]). In the second step, we applied an agglomerative hierarchical clustering method using the preclusters from step 1 as an input [21]. As we aimed to reproduce the subtypes described by Ferreira et al. [18], the number of clusters was constrained to four. To test whether the clusters indeed resembled the expected subtypes, we standardized the posterior and frontal thicknesses and the hippocampal volume measures (z = 0 represents the mean of the entire group) and examined the relative impairment of these three variables for each cluster (Fig. 1B). Cluster 1 (n = 70) showed negative z-scores

(representing greater neurodegeneration) on all MRI measures and was labeled “typical AD”. Cluster 2 (n = 77) was characterized by low hippocampal volumes but relatively preserved posterior and frontal thicknesses, thus labeled “limbic-predominant AD”. Cluster 3 (n = 76) showed the opposite pattern and was labeled “hippocampal-sparing AD”. Finally, cluster 4 (n = 37) showed relative preservation of all MRI measures and was labeled “mild atrophy AD”. Fig. 1C shows an exemplary MRI scan for each of the atrophy-defined AD subtypes.

2.8. Statistical analyses

Differences in baseline characteristics between atrophy-defined subtypes were assessed using analysis of variance with *post hoc* least squares difference tests for continuous variables and χ^2 and Kruskal-Wallis with *post hoc* Mann-Whitney U-tests for categorical or ordinal variables. To assess the degree of cortical thickness relative to that observed in cognitively normal persons, we standardized cortical thickness values of the atrophy-defined subtypes in medial and lateral temporal cortex, medial and lateral parietal cortex, and frontal and occipital cortex, based on the mean and standard deviation of 160 cognitively normal persons (mean age: 69.1 ± 9.5, 40.6% males, mean MMSE: 28.5 ± 1.6, 31.8% Aβ+) recruited from the same centers as described previously [8]. Then, we assessed differences between the atrophy-defined subtypes on [^{18}F]flortaucipir PET, WMH volumes and longitudinal change on MMSE. For [^{18}F]flortaucipir PET, we performed voxel-wise contrasts between the subtypes using SPM12. Furthermore, we compared SUVRs in seven predefined ROIs using analysis of variance with post-hoc least-squares difference tests. For WMH volumes, a generalized linear model with gamma family distribution and log link was used to account for the skewness of the data distribution, and the statistical models were corrected for age, sex, and center and total intracranial volume. [^{18}F]Flortaucipir PET ROI and WMH volume analyses were repeated by additionally adjusting for MMSE to account for potential confounding effects of disease severity. Finally, to examine clinical progression, we used MMSE scores as an outcome variable in linear mixed models with subtype, time, and subtype*time as predictors, while covarying for age, sex, and education. The models contained random intercept and slopes. The threshold for statistical significance was set at $P < .05$.

2.9. Data availability

Anonymized data will be shared by request from any qualified investigator for the sole purpose of replicating procedures and results presented in the manuscript and as long as data transfer is in agreement with European Union legislation on the General Data Protection Regulation.

3. Results

3.1. Subject characteristics

Baseline characteristics are provided in Table 1. Patients with hippocampal-sparing AD were younger than all other subtypes, had a lower proportion of *APOE* ε4 carriers than patients with limbic-predominant AD, and included more females than the typical AD subtype. Typical patients with AD had lower MMSE scores than all other subtypes. The mild atrophy

group included a greater proportion of patients with MCI relative to AD dementia than all other subtypes. Cortical thickness z-scores of the atrophy-defined subtypes relative to cognitively normal persons are presented in Supplementary Table 2.

3.2. [^{18}F]Flortaucipir PET

Fig. 2A shows mean voxel-wise [^{18}F]flortaucipir SUVR images for each of the atrophy-defined subtypes. Voxel-wise contrasts showed that hippocampal-sparing had greater [^{18}F]flortaucipir uptake in lateral temporoparietal cortex, precuneus, posterior cingulate, premotor cortex, and dorsolateral prefrontal cortex than in patients with mild atrophy AD, with a slight left-hemisphere predominance (Fig. 2B; $P < .05$ family-wise-error [FWE] corrected). Typical patients with AD had greater [^{18}F]flortaucipir uptake than patients with mild atrophy AD in bilateral inferior and middle temporal cortices and left inferior parietal lobule (Fig. 2B; $P < .05$ FWE corrected). At a more liberal threshold ($P < .001$ uncorrected for multiple comparisons), patients with limbic-predominant AD showed greater [^{18}F]flortaucipir uptake than patients with mild atrophy AD in medial and lateral temporal cortex, putamen, and medial prefrontal cortex (Fig. 2B). Patients with hippocampal-sparing AD had greater [^{18}F]flortaucipir uptake than patients with limbic-predominant AD in temporal, parietal, and frontal cortex (left > right), but none of these effects survived FWE correction (data not shown). There were no significant differences for the other contrasts.

ROI analyses using PVC data (Fig. 3A) were largely in line with the voxel-wise results, as the highest cortical [^{18}F]flortaucipir uptake was found in patients with hippocampal-sparing (especially in frontoparietal regions) and typical (mainly in lateral temporal and occipital cortices) AD, followed by patients with limbic-predominant and then mild atrophy AD. The entorhinal cortex, however, showed greater entorhinal SUVR in patients with limbic-predominant AD than in all other subtypes ($P < .05$). Non-PVC data showed higher [^{18}F]flortaucipir uptake in patients with limbic-predominant AD than in patients with hippocampal-sparing ($P < .05$) and, at statistical trend-level, mild atrophy ($P = .055$) and typical ($P = .051$) AD and showed similar results in the remaining ROIs compared with PVC data (Supplementary Fig. 1). Results remained essentially the same when adjusting for MMSE to account for potential effects of disease severity (Supplementary Table 3).

3.3. White matter hyperintensity volumes

Table 2 and Fig. 3B show the regional WMH volume loadings for each of the atrophy-defined subtypes. Statistical analyses of lobar loading of WMH showed that typical patients with AD had greater temporal WMH volumes than all other subtypes and greater occipital WMH volumes than patients with hippocampal-sparing AD (Table 2). In terms of radially divided regions, the most periventricular regions appeared significantly more affected in typical AD than in all other subtypes (Table 2). There were no other significant differences between subtypes. Additional adjustment for MMSE attenuated differences in WMH volumes between subtypes, and the only contrast that remained significant was greater WMH volumes in periventricular regions in typical patients with AD than in those with hippocampal-sparing AD (Supplementary Table 4).

3.4. Clinical progression

Fig. 3C shows the slopes for MMSE scores over time, estimated from linear mixed models. The significant interaction time[3]subtype ($P < .05$) indicates that the cognitive trajectories differ across atrophy-defined subtypes. The hippocampal-sparing group showed the steepest slope (−2.6 [standard error: 0.4] MMSE points per year, $P < .001$), followed by the typical AD group (−2.0 [0.1], $P < .001$) and then the limbic-predominant (−1.5 [0.2], $P < .001$) and mild atrophy (−1.5 [0.3], $P = .141$) AD groups.

4. Discussion

We used a clustering method to in vivo replicate neuro-pathologically established subtypes of AD based on atrophy in medial temporal, posterior, and frontal brain regions of 260 patients who are Aβ-positive with prodromal AD or AD dementia and tested whether they differed on tau PET, WMH burden, and rate of cognitive decline. We found the greatest tau load in patients with hippocampal-sparing (neocortical-predominant) AD and typical (temporal-predominant) patients with AD, while the entorhinal cortex was especially implicated in the limbic-predominant group. In addition, typical patients with AD showed the most pronounced WMH load compared with the other subtypes. Patients with hippocampal-sparing AD showed the most rapid cognitive decline, followed by typical patients with AD. These findings suggest that structural MRI can be used to identify biologically and clinically meaningful subtypes of AD and that distinct tau PET patterns and white matter hyperintensities are associated with atrophy-defined subtypes.

A recent study used a clustering approach on entorhinal versus cortical tau PET uptake and showed that the resulting clusters were associated with different clinical presentations of AD [22]. A novelty of this study is our demonstration of distinct tau PET patterns in atrophy-defined subtypes of AD. Although patients with hippocampal-sparing AD and typical patients with AD both showed tau PET uptake in AD-specific temporoparietal regions (Fig. 2), the hippocampal-sparing subtype was characterized by a frontoparietal predominance (L > R), which is in line with the distribution of neurofibrillary tangle pathology found in postmortem studies [5], their often atypical “nonamnestic” disease presentation [23], and the lower frequency of *APOE* ε4-positivity [18]. Typical patients with AD, on the other hand, harbored most tau pathology in lateral temporal cortex areas. In line with earlier studies [24,25], they additionally had highest white matter hyperintensity volumes. Patients with limbic-predominant AD showed intermediate neocortical involvement but had the greatest uptake of all subtypes in the entorhinal cortex, corresponding to neuropathologically observed distribution of neurofibrillary tangle pathology [5]. The patients with relatively preserved gray matter (mild atrophy group) were the least affected by tau pathology. This group showed only subtle reductions in cortical thickness compared with cognitively normal persons (Supplementary Table 2) but were all Aβ+ and had objective cognitive deficits (i.e., MCI or AD dementia, mean MMSE: 24 ± 4). Potential explanations for this subtype include the possibility that this group is characterized by low cognitive resilience to brain pathology [26] or that pathological processes other than Aβ, tau, or atrophy are driving the clinical symptoms (e.g., vascular damage [other than WMH] or different proteinopathies [27]).

Altogether, our findings highlight that tau PET patterns map well onto the expected atrophy distribution and clinical phenotype [22,28–31]. Both in terms of global and regional burden, tau and (relative) atrophy often spatially coincided, illustrated by, for example, the elevated entorhinal cortex tau PET signal in patients with limbic-predominant atrophy, the low tau PET retention in patients who only showed mild atrophy, and the neocortical predominant tau PET pattern in patients with pronounced reductions in cortical thickness of posterior and frontal cortical regions but relatively preserved hippocampal volumes. Previous studies have consistently indicated that the distribution and extent of Aβ load has only a marginal effect on neurodegeneration and cognitive decline in clinical stages of AD [32–34]. Although the regional effect of Aβ (all patients in this study were Aβ+) on brain atrophy could not be examined (some patients had only cerebrospinal fluid available and different Aβ PET tracers were used), it is thus unlikely that the atrophy-defined subtypes can be explained by regional differences in Aβ pathology. Hence, the present study supports several other studies in demonstrating that tau pathology is closely associated with sites of neurodegeneration [12,28,35,36], and it could be argued that the inherent distribution of cerebral tau pathology determines to a large extent the AD subtype identified on structural MRI. The contribution of WMH volumes to the manifestation of atrophy-defined subtypes is less clear. Although this study—consistently with previous studies [18,25]—showed that typical patients with AD had the greatest WMH volume burden, it is unknown whether this originates from Wallerian degeneration as a response to hyperphosphorylated tau and/or Aβ or is due to small vessel disease. However, based on the observation that both WHM volumes and tau load were most pronounced in the temporal cortex in typical AD versus the other subtypes, one may speculate that the observed temporal WMH lesions were primarily due to Wallerian degeneration [37].

Strengths of the study include the large number of Aβ+ patients with AD with tau PET, MRI, and MMSE available. Furthermore, we used a quantitative implementation of well-established visual rating systems to capture a priori defined subtypes of AD. There are also several limitations. First, compared with other studies [1,5,18], we had an overrepresentation of limbic-predominant and especially hippocampal-sparing cases relative to typical patients with AD, possibly due to cohort effects, methodological aspects, or the relatively young mean age of the sample. However, group characteristics were largely in line with previous studies (e.g., younger age and *APOE* ε4 prevalence in hippocampal-sparing AD), suggesting that comparable subtypes were captured across studies. Second, based on the presumed temporal lag between tau spread and atrophy [35,38,39], the tau PET signal could have converged across MRI-defined subtypes and we may have underestimated actual differences in tau pathology. Third, we used different MRI scanners across centers. However, as our clustering approach was based on covariance patterns (including both relative increases and decreases) and not on actual differences, we argue that this had only minor effects on the clustering. Further outstanding issues are the possibility that some of the differences between subtypes are partly driven by differences in disease stage (as adjusting the WMH volume analyses for MMSE attenuated most of the regional differences between subtypes) or even that multiple subtypes are in reality on the same continuum of a single subtype. Longitudinal studies will be essential to further examine this. Other key topics for future research are to investigate the rates and distribution of brain atrophy, accumulation of tau,

and WMH and to test whether and how these are related to cognitive changes over time. It would also be important to postmortem verify the regional distribution of tau pathology that was observed using ante-mortem PET and to assess the extent of comorbid pathologies (e.g., TDP-43, α-synuclein) in the different subtypes that can currently not be detected by neuroimaging techniques.

Supplementary Material

Refer to Web version on PubMed Central for supplementary material.

Acknowledgments

Work at Lund University was supported by the European Research Council, the Swedish Research Council, the Marianne and Marcus Wallenberg foundation, the Knut and Alice Wallenberg foundation, the Strategic Research Area MultiPark (Multidisciplinary Research in Parkinson's disease) at Lund University, the Swedish Brain Foundation, the Swedish Alzheimer Foundation, The Parkinson Foundation of Sweden, The Parkinson Research Foundation, the Skåne University Hospital Foundation, and the Swedish federal government under the ALF agreement. Doses of ^{18}F-flutemetamol injection were sponsored by GE Healthcare. Work at UCSF was supported by National Institute on Aging grants (R01-AG045611, P50-AG023501, P01-AG19724, R01-AG038791, and U54-NS092089), the Alzheimer's Association (AARF-16-443577), Tau Consortium, and the Michael J Fox foundation. Work at Gangnam Severance Hospital was financially supported by the National Research Foundation of Korea (NRF) grant funded by the Korean government (MSIP, 2015R1C1A2A01054507) and Basic Science Research Program through the NRF funded by the Ministry of Science, ICT & Future Planning (2017R1A2B2006694). C.H.S. is funded by the Alzheimer's Society (AS-JF-17-011). For UCSF and the BioFINDER study, the precursor of [^{18}F]flortaucipir was provided by AVID radiopharmaceuticals.

Disclosures: O.H. has acquired research support (for the institution) from Roche, GE Healthcare, Biogen, AVID Radiopharmaceuticals, Fujirebio, and Euroimmun. In the past 2 years, he has received consultancy/speaker fees (paid to the institution) from Lilly, Roche, and Fujirebio. A.L.B. receives research support from NIH U54NS092089, R01AG031278, R01AG038791, R01AG032306, R01AG022983, the Tau Research Consortium, the Bluefield Project to Cure Frontotemporal Dementia, Corticobasal Degeneration Solutions, and the Alzheimer's Association. He has served as a consultant for Abbvie, Amgen, Celgene, Ionis, Janssen, Merck, UCB, and Toyama and received research support from Avid, Biogen, BMS, C2N, Cortice, Forum, Genentech, Janssen, Pfizer, Eli Lilly, Roche, and TauRx, He holds stock options in Aeton, Alector, and Delos. G.D.R. receives research support from Avid Radiopharmaceuticals/Eli Lilly, GE Healthcare, and Piramal. He has received speaking honoraria or consulting fees from Eisai, Genentech, Lundbeck, Merck, Putnam, and Roche. B.L.M. is the Medical Director for John Douglas French Foundation; Scientific Director for the Tau Consortium; Director/Medical Advisory Board of the Larry L. Hillblom Foundation; Scientific Advisory Board Member for the National Institute for Health Research Cambridge Biomedical Research Centre and its subunit, the Biomedical Research Unit in Dementia (UK); and Board Member for the American Brain Foundation. The other authors report no conflicts of interest.

References

[1]. Risacher SL, Anderson WH, Charil A, Castelluccio PF, Shcherbinin S, Saykin AJ, et al. Alzheimer disease brain atrophy subtypes are associated with cognition and rate of decline. Neurology 2017;89:2176–86. [PubMed: 29070667]

[2]. Zhang X, Mormino EC, Sun N, Sperling RA, Sabuncu MR, Yeo BT, et al. Bayesian model reveals latent atrophy factors with dissociable cognitive trajectories in Alzheimer's disease. Proc Natl Acad Sci U S A 2016;113:E6535–44. [PubMed: 27702899]

[3]. Dong A, Toledo JB, Honnorat N, Doshi J, Varol E, Sotiras A, et al. Heterogeneity of neuroanatomical patterns in prodromal Alzheimer's disease: links to cognition, progression and biomarkers. Brain 2017; 140:735–47. [PubMed: 28003242]

[4]. Ten Kate M, Dicks E, Visser PJ, van der Flier WM, Teunissen CE, Barkhof F, et al. Atrophy subtypes in prodromal Alzheimer's disease are associated with cognitive decline. Brain 2018;141:3443–56. [PubMed: 30351346]

[5]. Murray ME, Graff-Radford NR, Ross OA, Petersen RC, Duara R, Dickson DW. Neuropathologically defined subtypes of Alzheimer's disease with distinct clinical characteristics: a retrospective study. Lancet Neurol 2011;10:785–96. [PubMed: 21802369]

[6]. Whitwell JL, Dickson DW, Murray ME, Weigand SD, Tosakulwong N, Senjem ML, et al. Neuroimaging correlates of pathologically defined subtypes of Alzheimer's disease: a case-control study. Lancet Neurol 2012;11:868–77. [PubMed: 22951070]

[7]. Lehmann M, Ghosh PM, Madison C, Laforce R Jr, Corbetta-Rastelli C, Weiner MW, et al. Diverging patterns of amyloid deposition and hypometabolism in clinical variants of probable Alzheimer's disease. Brain 2013;136:844–58. [PubMed: 23358601]

[8]. Ossenkoppele R, Rabinovici GD, Smith R, Cho H, Scholl M, Strandberg O, et al. Discriminative accuracy of [18F]flortaucipir positron emission tomography for Alzheimer disease vs other neurodegenerative disorders. JAMA 2018;320:1151–62. [PubMed: 30326496]

[9]. Albert MS, DeKosky ST, Dickson D, Dubois B, Feldman HH, Fox NC, et al. The diagnosis of mild cognitive impairment due to Alzheimer's disease: recommendations from the National Institute on Aging-Alzheimer's Association workgroups on diagnostic guidelines for Alzheimer's disease. Alzheimers Dement 2011;7:270–9. [PubMed: 21514249]

[10]. McKhann GM, Knopman DS, Chertkow H, Hyman BT, Jack CR Jr, Kawas CH, et al. The diagnosis of dementia due to Alzheimer's disease: recommendations from the National Institute on Aging-Alzheimer's Association workgroups on diagnostic guidelines for Alzheimer's disease. Alzheimers Dement 2011;7:263–9. [PubMed: 21514250]

[11]. Cho H, Choi JY, Hwang MS, Kim YJ, Lee HM, Lee HS, et al. In vivo cortical spreading pattern of tau and amyloid in the Alzheimer disease spectrum. Ann Neurol 2016;80:247–58. [PubMed: 27323247]

[12]. Ossenkoppele R, Schonhaut DR, Scholl M, Lockhart SN, Ayakta N, Baker SL, et al. Tau PET patterns mirror clinical and neuroanatomical variability in Alzheimer's disease. Brain 2016;139:1551–67. [PubMed: 26962052]

[13]. Mattsson N, Scholl M, Strandberg O, Smith R, Palmqvist S, Insel PS, et al. 18F-AV-1451 and CSF T-tau and P-tau as biomarkers in Alzheimer's disease. EMBO Mol Med 2017;9:1212–23. [PubMed: 28743782]

[14]. Maass A, Landau S, Baker SL, Horng A, Lockhart SN, La Joie R, et al. Comparison of multiple tau-PET measures as biomarkers in aging and Alzheimer's disease. Neuroimage 2017;157:448–63. [PubMed: 28587897]

[15]. Rousset OG, Ma Y, Evans AC. Correction for partial volume effects in PET: principle and validation. J Nucl Med 1998;39:904–11. [PubMed: 9591599]

[16]. Swedish BioFINDER study, Scholl M, Ossenkoppele R, Strandberg O, Palmqvist S, Jogi J, Ohlsson T, et al. Distinct 18F-AV-1451 tau PET retention patterns in early- and late-onset Alzheimer's disease. Brain 2017;140:2286–94. [PubMed: 29050382]

[17]. Sudre CH, Cardoso MJ, Bouvy WH, Biessels GJ, Barnes J, Ourselin S. Bayesian model selection for pathological neuroimaging data applied to white matter lesion segmentation. IEEE Trans Med Imaging 2015; 34:2079–102. [PubMed: 25850086]

[18]. Ferreira D, Verhagen C, Hernandez-Cabrera JA, Cavallin L, Guo CJ, Ekman U, et al. Distinct subtypes of Alzheimer's disease based on patterns of brain atrophy: longitudinal trajectories and clinical applications. Sci Rep 2017;7:46263. [PubMed: 28417965]

[19]. Ferreira D, Cavallin L, Larsson EM, Muehlboeck JS, Mecocci P, Vellas B, et al. Practical cut-offs for visual rating scales of medial temporal, frontal and posterior atrophy in Alzheimer's disease and mild cognitive impairment. J Intern Med 2015;278:277–90. [PubMed: 25752192]

[20]. Banfield JD, Raftery AE. Model-based Gaussian and non-Gaussian clustering. Biometrics 1993;49:803–21.

[21]. Zhang T, Ramakrishnon R, Livny M. BIRCH: an efficient data clustering method for very large databases. In: Proceedings of the ACM SIGMOD Conference on Management of Data Montreal, Canada; 1996 p. 103–14.

[22]. Whitwell JL, Graff-Radford J, Tosakulwong N, Weigand SD, Machulda M, Senjem ML, et al. [^{18}F]AV-1451 clustering of entorhinal and cortical uptake in Alzheimer's disease. Ann Neurol 2018;83:248–57. [PubMed: 29323751]

[23]. Ossenkoppele R, Cohn-Sheehy BI, La Joie R, Vogel JW, Moller C, Lehmann M, et al. Atrophy patterns in early clinical stages across distinct phenotypes of Alzheimer's disease. Hum Brain Mapp 2015; 36:4421–37. [PubMed: 26260856]

[24]. Ferreira D, Shams S, Cavallin L, Viitanen M, Martola J, Granberg T, et al. The contribution of small vessel disease to subtypes of Alzheimer's disease: a study on cerebrospinal fluid and imaging biomarkers. Neurobiol Aging 2018;70:18–29. [PubMed: 29935417]

[25]. Park JY, Na HK, Kim S, Kim H, Kim HJ, Seo SW, et al. Robust Identification of Alzheimer's disease subtypes based on cortical atrophy patterns. Sci Rep 2017;7:43270. [PubMed: 28276464]

[26]. Stern Y, Arenaza-Urquijo EM, Bartres-Faz D, Belleville S, Cantilon M, Chetelat G, et al. Whitepaper: defining and investigating cognitive reserve, brain reserve, and brain maintenance. Alzheimers Dement 2018; 10.1016/j.jalz.2018.07.219.

[27]. Nelson PT, Dickson DW, Trojanowski JQ, Jack CR, Boyle PA, Arfanakis K, et al. Limbic-predominant age-related TDP-43 encephalopathy (LATE): consensus working group report. Brain 2019; 142:1503–27. [PubMed: 31039256]

[28]. Xia C, Makaretz SJ, Caso C, McGinnis S, Gomperts SN, Sepulcre J, et al. Association of in vivo [18F]AV-1451 tau PET imaging results with cortical atrophy and symptoms in typical and atypical Alzheimer disease. JAMA Neurol 2017;74:427–36. [PubMed: 28241163]

[29]. Dronse J, Fliessbach K, Bischof GN, von Reutern B, Faber J, Hammes J, et al. In vivo patterns of tau pathology, amyloid-beta burden, and neuronal dysfunction in clinical variants of Alzheimer's disease. J Alzheimers Dis 2017;55:465–71. [PubMed: 27802224]

[30]. Mattsson N, Insel PS, Donohue M, Jogi J, Ossenkoppele R, Olsson T, et al. Predicting diagnosis and cognition with (18)F-AV-1451 tau PET and structural MRI in Alzheimer's disease. Alzheimers Dement 2019; 15:570–80. [PubMed: 30639421]

[31]. Ossenkoppele R, Smith R, Ohlsson T, Strandberg O, Mattsson N, Insel PS, et al. Associations between tau, Abeta, and cortical thickness with cognition in Alzheimer disease. Neurology 2019;92:e601–12. [PubMed: 30626656]

[32]. Rabinovici GD, Furst AJ, Alkalay A, Racine CA, O'Neil JP, Janabi M, et al. Increased metabolic vulnerability in early-onset Alzheimer's disease is not related to amyloid burden. Brain 2010;133:512–28. [PubMed: 20080878]

[33]. Ossenkoppele R, Zwan MD, Tolboom N, van Assema DM, Adriaanse SF, Kloet RW, et al. Amyloid burden and metabolic function in early-onset Alzheimer's disease: parietal lobe involvement. Brain 2012;135:2115–25. [PubMed: 22556189]

[34]. Altmann A, Ng B, Landau SM, Jagust WJ, Greicius MD. Alzheimer's disease neuroimaging I. Regional brain hypometabolism is unrelated to regional amyloid plaque burden. Brain 2015;138:3734–46. [PubMed: 26419799]

[35]. Iaccarino L, Tammewar G, Ayakta N, Baker SL, Bejanin A, Boxer AL, et al. Local and distant relationships between amyloid, tau and neurodegeneration in Alzheimer's disease. Neuroimage Clin 2018; 17:452–64. [PubMed: 29159058]

[36]. Tetzloff KA, Graff-Radford J, Martin PR, Tosakulwong N, Machulda MM, Duffy JR, et al. Regional distribution, asymmetry, and clinical correlates of tau uptake on [18F]AV-1451 PET in atypical Alzheimer's disease. J Alzheimers Dis 2018;62:1713–24. [PubMed: 29614676]

[37]. McAleese KE, Walker L, Graham S, Moya ELJ, Johnson M, Erskine D, et al. Parietal white matter lesions in Alzheimer's disease are associated with cortical neurodegenerative pathology, but not with small vessel disease. Acta Neuropathol 2017;134:459–73. [PubMed: 28638989]

[38]. Jack CR Jr, Wiste HJ, Schwarz CG, Lowe VJ, Senjem ML, Vemuri P. et al. Longitudinal tau PET in ageing and Alzheimer's disease. Brain 2018;141:1517–28. [PubMed: 29538647]

[39]. Harrison TM, La Joie R, Maass A, Baker SL, Swinnerton K, Fenton L, et al. Longitudinal tau accumulation and atrophy in aging and Alzheimer disease. Ann Neurol 2019;85:229–40. [PubMed: 30597624]

RESEARCH IN CONTEXT

1. Systematic review: Previous studies have used structural MRI to identify distinct subtypes of Alzheimer's disease (AD). The underlying tau PET pattern of these AD subtypes is currently unknown.
2. Interpretation: Our results demonstrate distinct tau PET patterns across hippocampal-sparing (frontoparietal predominant), limbic-predominant (medial temporal lobe predominant) and typical (temporal predominant) atrophy-defined subtypes of AD.
3. Future directions: To evaluate the natural evolution of distinct AD subtypes in terms of tau PET accumulation, brain atrophy and decline in domain-specific cognitive functions, and test whether information on AD subtype informs clinicians (e.g. prognosis) or clinical trial design (e.g. selection or monitoring).

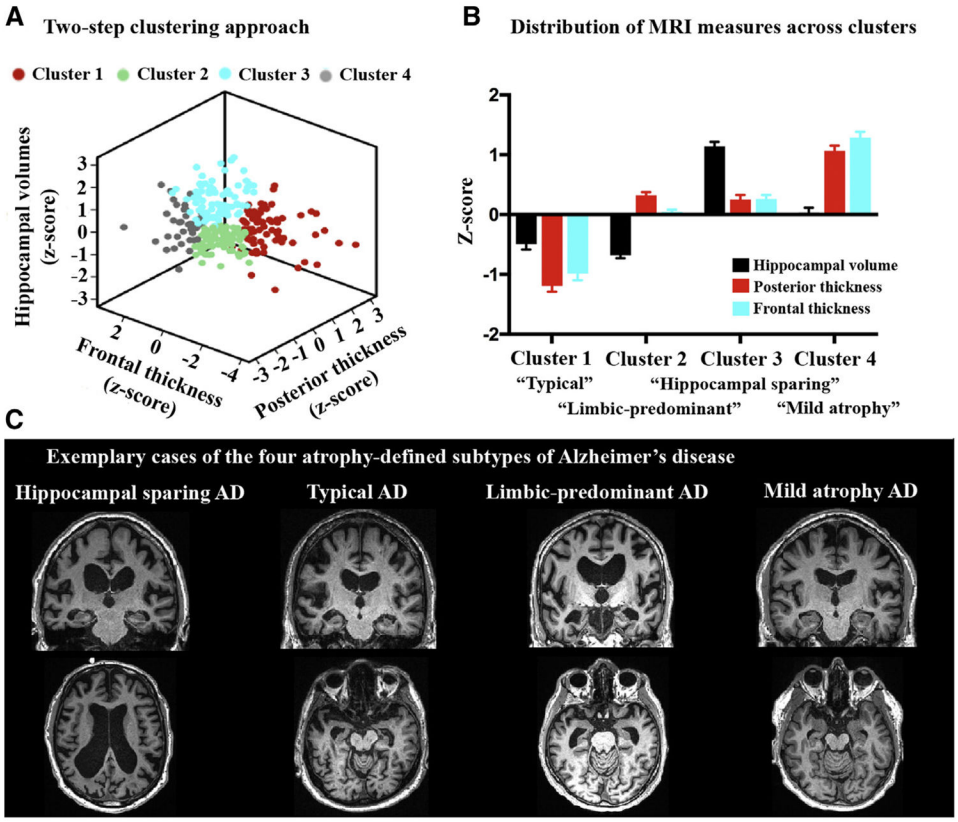

Fig. 1.

Clustering method for determining atrophy-defined subtypes of AD. We first performed a two-step clustering algorithm (constrained to k = 4) with hippocampal volumes, posterior thickness (occipital and parietal cortex combined), and frontal thickness as input (A). Then the continuous MRI measures were transformed to z-scores across the sample (B). This revealed groups with overall low z-scores (cluster 1, called "atypical AD"), low hippocampal volumes but preserved cortical measures (cluster 2, "limbic-predominant AD"), the opposite pattern (cluster 3, "hippocampal sparing AD"), and a relatively spared group (cluster 4, "mild atrophy AD"). (C) A coronal and axial slice for an exemplary case from each of the four atrophy-defined subtypes. Abbreviations: AD, Alzheimer's disease; MRI, magnetic resonance imaging.

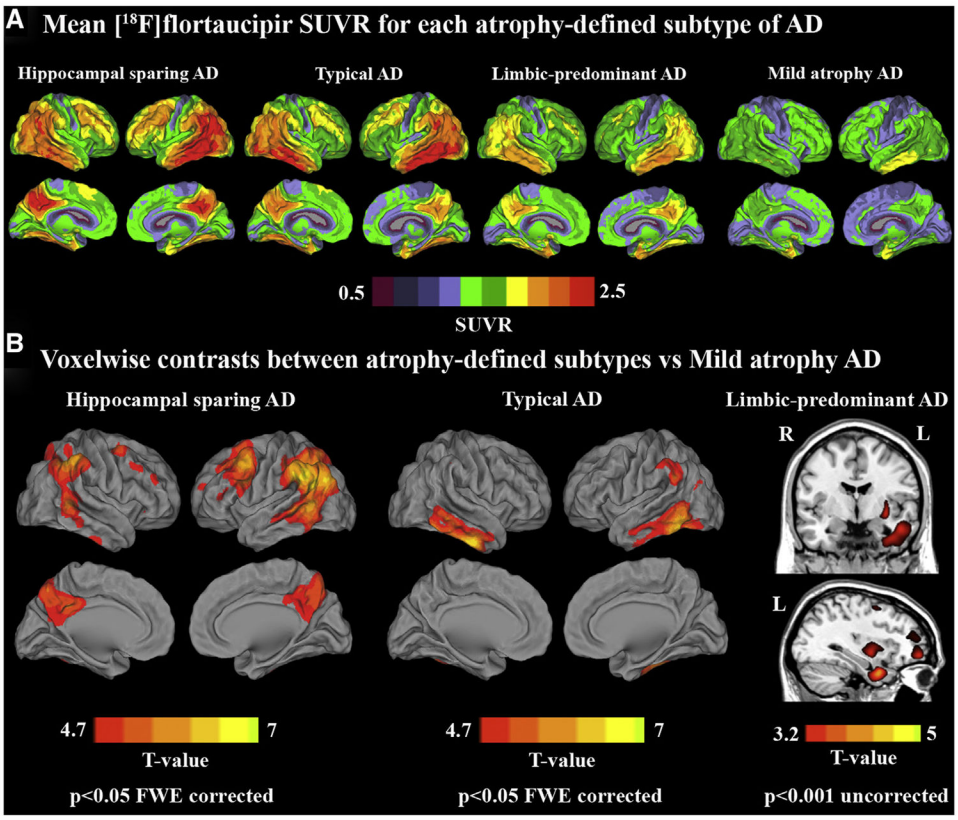

Fig. 2.

[18F]Flortaucipir uptake patterns by atrophy-defined subtypes of Alzheimer's disease. (A) Mean voxel-wise [18F]flortaucipir SUVR images for the four atrophy-defined subtypes of Alzheimer's disease. (B) Voxel-wise contrast between hippocampal-sparing AD (left), typical AD (middle), and limbic-predominant AD (right) versus patients with mild atrophy AD. Abbreviations: AD, Alzheimer's disease; FWE, family-wise error; SUVR, standardized uptake value ratio.

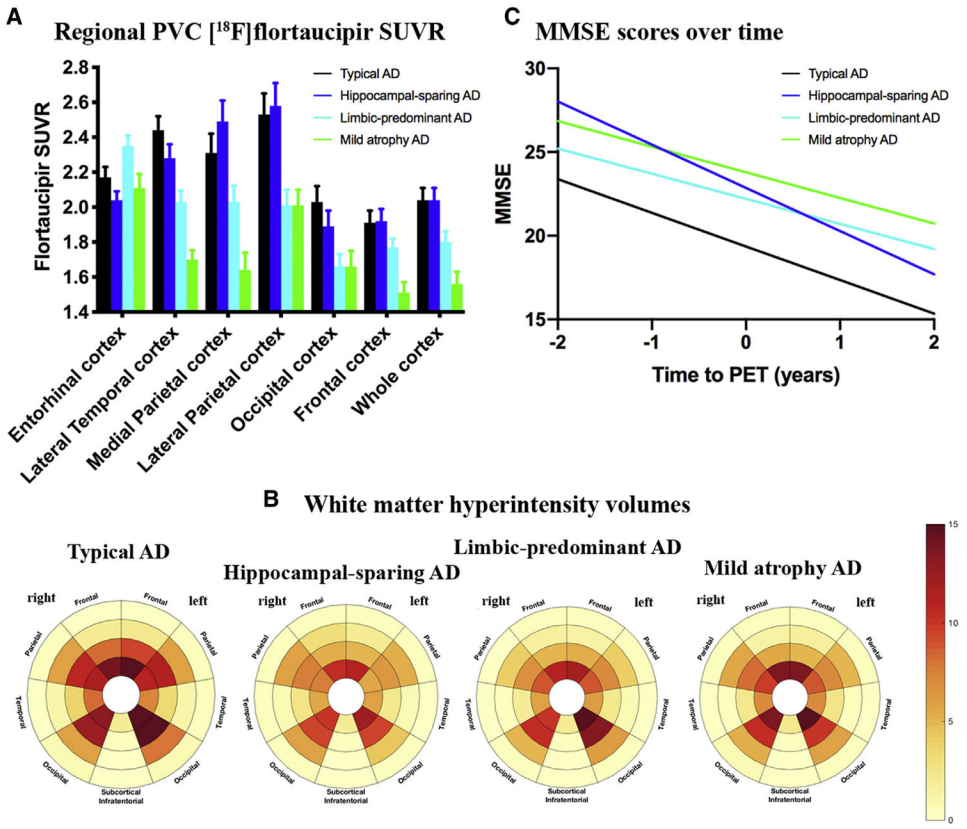

Fig. 3.

Tau PET, white matter hyperintensity volumes, and clinical progression by atrophy-defined subtypes of Alzheimer's disease. (A) Partial volume–corrected [^{18}F]flortaucipir SUVRs in seven predefined regions-of-interest for the four atrophy-defined subtypes of Alzheimer's disease. Entorhinal cortex: Limbic-predominant > HC-sparing, $P < .001$; Limbic-predominant > Typical & Mild, $P < .05$. Lateral temporal cortex: HC-sparing > Mild, $P < .001$; HC-sparing > Limbic-predominant, $P < .05$; Typical > Mild & Limbic-predominant, $P < .001$; Limbic-predominant > mild, $P < .05$. Medial parietal cortex: HC-sparing > Mild, $P < .001$; HC-sparing > Limbic-predominant, $P < .01$; Typical > Mild, $P < .001$; Limbic-predominant > mild, $P < .05$. Lateral parietal cortex: HC-sparing > Mild, & Limbic-predominant, $P < .001$; Typical > Mild, $P < .001$; Typical > Limbic-predominant, $P < .01$. Occipital cortex: HC-sparing > Mild, $P < .01$; HC-sparing > Limbic-predominant, $P < .05$; Typical > Mild & Limbic-predominant, $P < .01$. Frontal cortex: HC-sparing > Mild, $P < .001$; Typical > Mild, $P < .001$; Limbic-predominant > Mild, $P < .05$. Whole-cortex: HC-sparing > Mild, $P < .001$; HC-sparing > Limbic-predominant, $P < .01$; Typical > Mild, $P < .001$; Typical > Limbic-predominant, $P < .01$; Limbic-predominant > Mild, $P < .05$. (B) Bullseye plots displaying regional spread of white matter hyperintensity volumes. The concentric rings of the plot represent four equidistant layers of white matter (center = periventricular and outer layer = juxtacortical). (C) The slopes for MMSE scores over time as estimated by linear mixed models. Abbreviations: AD, Alzheimer's disease; MMSE,

Mini-Mental State Examination; SUVR, Standardized uptake value ratio; PVC, partial volume corrected.

Table 1

Patient characteristics by atrophy-defined subtype

Variable	Typical AD (n = 70)	Hippocampal-sparing AD (n = 76)	Limbic-predominant AD (n = 77)	Mild atrophy AD (n = 37)	All (n = 260)
Age [*]	69.1 ± 9.5	64.6 ± 9.1	72.0 ± 9.6	69.2 ± 9.4	69.2 ± 9.5
Sex (% male) [†]	55.7	34.2	46.8	37.8	44.2
Education (years)	13.4 ± 4.6	14.1 ± 4.3	12.5 ± 5.3	12.1 ± 5.4	13.2 ± 4.9
MMSE [‡]	19.6 ± 6.2	22.9 ± 5.6	22.0 ± 4.7	24.1 ± 3.6	21.9 ± 5.5
CDR [§]	1.2 ± 0.7	0.7 ± 0.3	0.9 ± 0.5	0.6 ± 0.2	0.9 ± 0.5
APOE ε4 positivity [¶]	59.0% (36/61)	48.5% (33/68)	65.6% (42/64)	50.0% (17/34)	56.4% (128/227)
APOE genotype	10 ε4/ε4 (16%)	7 ε4/ε4 (10%)	14 ε4/ε4 (22%)	8 ε4/ε4 (24%)	39 ε4/ε4 (17%)
	23 ε3/ε4 (38%)	25 ε3/ε4 (37%)	27 ε3/ε4 (42%)	9 ε3/ε4 (36%)	84 ε3/ε4 (37%)
	25 ε3/ε3 (41%)	34 ε3/ε3 (50%)	19 ε3/ε3 (30%)	16 ε3/ε3 (47%)	94 ε3/ε3 (41%)
	3 ε2/ε4 (5%)	1 ε2/ε4 (1%)	1 ε2/ε4 (3%)	0 ε2/ε4 (0%)	5 ε2/ε4 (2%)
	0 ε2/ε3 (0%)	1 ε2/ε3 (1%)	3 ε2/ε3 (5%)	1 ε2/ε3 (3%)	5 ε2/ε3 (2%)
Diagnosis [#] (MCI/AD dementia)	14/56	25/51	23/54	21/16	83/177
Center (n, Seoul/Lund/UCSF)	11/47/12	22/8/46	43/17/17	19/7/11	95/79/86

Abbreviations: MMSE, Mini-Mental state examination; CDR, Clinical Dementia Rating scale; *APOE*, apolipoprotein E; MCI, mild cognitive impairment; AD, Alzheimer's disease; UCSF, University of California San Francisco.

[*] Hippocampal sparing AD < Typical AD/Limbic-predominant AD/Mild atrophy AD, $P < .05$.

[†] Typical AD > (males) Hippocampal-sparing AD, $P < .01$.

[‡] Typical AD < Hippocampal sparing AD/Limbic-predominant AD/Mild atrophy AD, $P < .05$.

[§] Typical AD > Hippocampal sparing AD/Limbic-predominant AD/Mild atrophy AD & Limbic-predominant AD > Hippocampal sparing AD/Mild atrophy AD, $P < .05$.

[¶] Limbic-predominant AD > Hippocampal sparing AD, $P < .05$.

[#] Typical AD/Hippocampal sparing AD/Limbic-predominant AD > (dementia patients) Mild atrophy AD, $P < .05$.

Table 2

White matter hyperintensity volumes for each atrophy-defined subtype of Alzheimer's disease

Region-of-interest	Typical AD	Hippocampal-sparing AD	Limbic-predominant AD	Mild atrophy AD
Total	8.58 [6.65–10.52]	6.15 [4.37–7.94]	6.33 [5.01–7.65]	6.49 [4.42–8.57]
Frontal	4.09 [3.01–5.18]	3.05 [2.17–3.93]	3.03 [2.34–3.72]	3.06 [2.17–3.95]
Parietal	2.29 [1.58–2.99]	1.59 [0.89–2.29]	1.64 [1.15–2.14]	1.93 [0.85–3.00]
Occipital	1.04 [0.81–1.27]*	0.70 [0.52–0.88]	0.84 [0.66–1.02]	0.76 [0.57–0.94]
Temporal	1.00 [0.76–1.25]†	0.65 [0.45–0.85]	0.68 [0.54–0.82]	0.61 [0.46–0.77]
Basal ganglia	0.19 [0.13–0.25]	0.17 [0.13–0.21]	0.16 [0.13–0.20]	0.21 [0.14–0.28]
Periventricular	2.56 [2.16–2.96]‡	1.60 [1.28–1.92]	1.88 [1.59–2.17]	1.88 [1.50–2.27]
Medial	5.09 [3.67–6.52]§	3.47 [2.20–4.74]	3.34 [2.47–4.21]	3.34 [2.02–4.65]
Peripheral	1.12 [0.79–1.46]	1.19 [0.78–1.60]	1.10 [0.81–1.38]	1.25 [0.78–1.71]

NOTE. Values represent marginal mean [95% confidence interval] white matter hyperintensity volumes (mL) after correction for age, sex, total intracranial volume, and center. *P* values are based on Wald T-tests.

Abbreviation: AD, Alzheimer's disease.

*Typical AD > Hippocampal sparing AD, $P < .05$.

†Typical AD > mild atrophy AD, $P < .01$ & Typical AD > Hippocampal sparing AD and Limbic-predominant AD, $P < .05$.

‡Typical AD > Hippocampal sparing AD and Limbic-predominant AD, $P < .01$ & Typical AD > mild atrophy AD, $P < .05$.

§Typical AD > Limbic-predominant AD, $P < .05$.